Chemical Science

ROYAL SOCIETY OF CHEMISTRY

EDGE ARTICLE

View Article Online
View Journal | View Issue

Open Access Article. Published on 29 August 2025. Downloaded on 1/22/2026 7:31:51 AM.
This article is licensed under a Creative Commons Attribution-NonCommercial 3.0 Unported Licence.

Check for updates

Cite this: *Chem. Sci.*, 2025, **16**, 17298

All publication charges for this article have been paid for by the Royal Society of Chemistry

The "sweet spot" in length for contorted conjugated ladders in ultrafast-charging Li and Mg batteries

Wenrui Lei, † Kelsey Harrison, † Si Tong Bao, Kyunam Lee, Michael L. Steigerwald, Qian Cheng,* Nicholas M. Orchanian, * Colin Nuckolls * and Qifeng Jiang *

Received 2nd July 2025
Accepted 19th August 2025

DOI: 10.1039/d5sc04900h

rsc.li/chemical-science

Here, we explore a conjugated, contorted polymer framework tailored for ultrafast-rate charging/discharging, leveraging a tunable synthetic strategy to control its molecular length. We systematically explore the helical perylene diimide (hPDI) ladder polymers across three length regimes, short, medium, and long, to determine the optimal electrochemical stability and performance. The intermediate-length polymer strikes a critical balance between electrode integrity, solubility, and rate capability. Its reversible redox activity and structural robustness make it well-suited for both Li^+ and Mg^{2+} ions. The **hPDI-medium** cathode delivers a remarkable specific power of 22.4 kW kg^{-1} after 10 000 cycles in Li batteries and 1.7 kW kg^{-1} after 3000 cycles in Mg batteries, and we extend this to practically relevant mass loadings. This study highlights the critical role of molecular engineering in the rational design of high-performance organic cathode materials for sustainable energy storage.

Introduction

To develop sustainable solutions for escalating energy demands, it is imperative to find cost-effective and abundant materials for high performance batteries. Organic electrode materials (OEMs), comprising abundant elements, are poised to meet this demand with potential to decrease the overall CO_2 footprint for batteries while also showing improved compatibility with multivalent ion systems.[1–6] Overcoming the major limitations of inorganic materials, organic conjugated polymers with redox-active subunits have emerged as especially promising OEM candidates for cathodes in Li batteries because they can exceed the short cycle life of small molecules dissolved in liquid electrolyte.[7–9] Expanding beyond Li, divalent systems such as Mg offer a compelling anode alternative to pair with OEM cathodes due to the natural abundance and safety of Mg, along with the potential for higher volumetric energy density.[10–13] However, Mg battery chemistry presents significant challenges, particularly in achieving fast charge transport and electrode stability. These properties are especially desirable for applications such as electric aviation requiring intermittent high discharge capacity for short periods of time.[14–17]

We focused previously on atomically defined helical perylene diimide (hPDI) oligomers up to six PDI subunits in length as OEMs. The oligomer with six PDI subunits in length is named **hPDI-short**.[18] Several design elements emerged from these studies, enabling fast-charging and long-lifetime cathodes with Li-metal anodes and liquid electrolyte: (1) molecular contortion provided by the ladder backbone facilitates rapid ion transport. (2) The longer, conjugated structures have higher electronic conductivity, further boosting performance. This initial study highlighted improvements in cathode performance as a function of increasing ladder length, but the iterative synthetic procedure precluded extension of these oligomers to high-molecular weight systems, which could provide deeper insight into structure–property relationships and a higher-performing OEM.

Our new high-yielding synthesis allows us to test, for the first time, longer versions of the hPDI series. We synthesize two polymers: **hPDI-medium** (~15 PDI subunits) and **hPDI-long** (~90 PDI subunits). These new polymers exhibit ultrafast-charging capability as cathodes in both Li-metal batteries and Mg-metal batteries (Fig. 1). Controlling the degree of polymerization allows us to assess how ladder length influences battery performance. We identify a "sweet spot" in ladder length, exhibiting optimal ultrafast-charging and improved long-term stability in Li and Mg electrolyte systems (Fig. S1–S3). **hPDI-medium** demonstrates minimal capacity decay at rates up to 50 C in Li cells and delivers an impressive specific power of 22.4 kW kg^{-1} after 10 000 cycles, with an energy density of 235 Wh kg^{-1}. **hPDI-medium** overcomes the typical sluggish kinetics and electrode instability associated with Mg ions, having excellent capacity retention at rates up to 20 C, and

Department of Chemistry, Columbia University, New York, NY 10027, USA. E-mail: cn37@columbia.edu; qj2175@columbia.edu

† Both authors contributed equally to this work.

© 2025 The Author(s). Published by the Royal Society of Chemistry

Open Access Article. Published on 29 August 2025. Downloaded on 1/22/2026 7:31:51 AM.
This article is licensed under a Creative Commons Attribution-NonCommercial 3.0 Unported Licence.

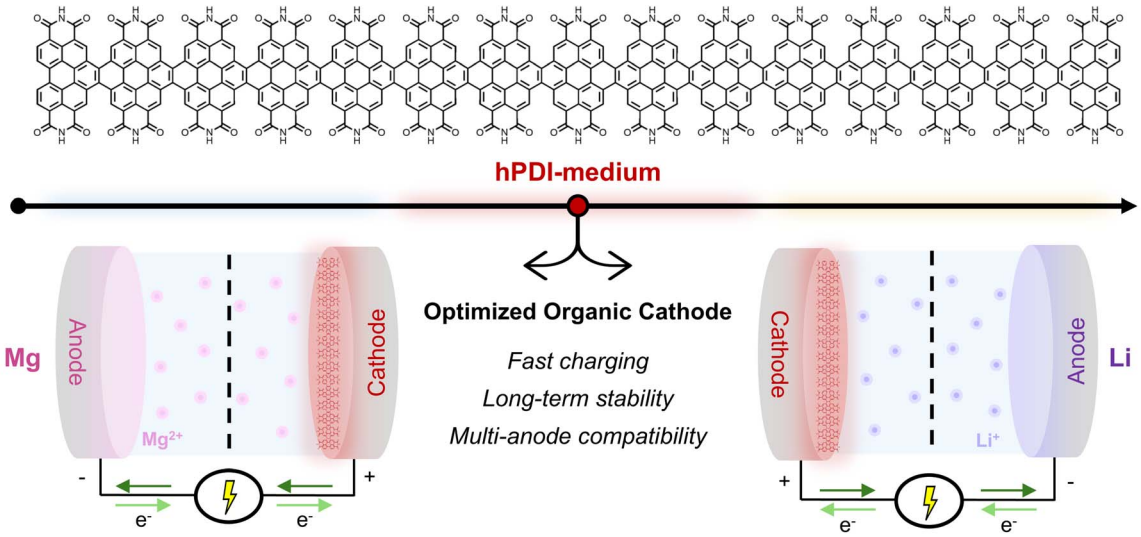

Fig. 1 **hPDI-medium** is a contorted ladder polymer, forming a cathode for Mg and Li-metal batteries.

delivers a specific power of 1.7 kW kg^{-1} and energy density of 65 Wh kg^{-1} after 3000 cycles.

Results and discussion

The synthesis yields defect-free hPDI ladders of tunable length (Fig. 2). A room-temperature Stille polymerization between di-brominated perylene tetraester (PTE-Br_2) and bi-s(tributylstannyl)acetylene is followed by an iodine-mediated photocyclization, yielding hPTRs. The aromatic resonances in the ^{1}H-NMR spectra of hPTRs reveal fully fused, defect-free conjugated backbones.[19] We vary the length of polymeric hPTRs by adjusting the molar ratio of monofunctional PTE-Br end-cap. We synthesized ladder polymers of "medium" length (averaging 15 PDI subunits) and "long" length (averaging 90 PDI subunits). We determine the polymer length by end group analysis using ^{1}H-NMR. Finally, the tetraesters were converted quantitatively into **hPDI-medium** and **hPDI-long** by imidization followed by vacuum thermolysis. TGA and IR-spectroscopy confirm the fidelity of this process and the presence of primary imides (Fig. S4 and S5). Powder X-ray diffraction reveals weak π–π interaction of the hPDI polymers (Fig. S6). This method greatly improves the scalability of these ladder polymers. Their extended ladder-type conjugation and molecular contortion along with primary imides provide high ionic and electronic conductivity.

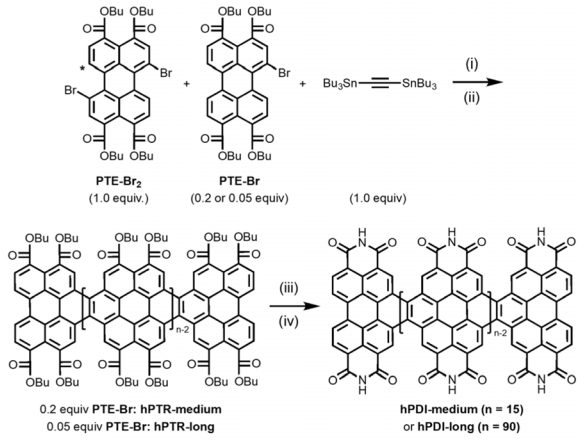

Fig. 2 Synthesis of **hPDI-medium** and **hPDI-long**. (i) Pd-P(*t*-Bu)$_3$-G4, K_3PO_4, toluene, rt, 24 hours. *Mixture of regioisomers. (ii) I_2, PhCl, hν, 72 hours. (iii) 6-aminoundecane, $Zn(OAc)_2$, imidazole, 160 °C, 24 hours. (iv) Vacuum, 360 °C, 2 hours.

Next, we assemble Li and Mg cells with the hPDI-*n* cathode series to evaluate their battery performance. Cyclic voltammetry shows the highly reversible redox activity expected for PDI subunits in the voltage range of 1.5–3.3 V *vs.* Li/Li^+ and 0.7–2.3 V *vs.* Mg/Mg^{2+} (Fig. S7–S9).[20–22] The resulting *b*-values indicate charge/discharge is a capacitive-controlled ($b = 1$) process for all hPDI-*n* polymers in the Li system, while stronger coulombic interactions of the divalent Mg ion give rise to mixed diffusion and capacitive-controlled ($0.5 < b < 1$) processes for **hPDI-short** and **hPDI-medium** in the Mg system. Interestingly, higher *b*-values ($0.9 < b < 1$) for **hPDI-long** in the Mg system indicate a predominantly capacitive-controlled process.[23,24]

Galvanostatic cycling tests demonstrate excellent rate capability for both Li and Mg-metal batteries (Fig. 3 and Table 1). In Li cells with a 1,3-dioxolane/1,2-dimethoxyethane (DME)-based electrolyte, **hPDI-medium** delivers the highest initial capacity of 110 mA h g^{-1} at 1 C (1 C = 0.13 A g^{-1}), when compared to the other ladder lengths, and retains remarkably high capacity retention (91%) under ultrafast-charging, up to 50 C (Fig. 3a and b). **hPDI-short** shows similar performance to **hPDI-medium**, delivering an initial capacity of 107 mA h g^{-1} and retaining 86% of its capacity up to 50 C. The longest ladder of the series, **hPDI-long**, maintains the best capacity retention (94%) at 50 C, but only delivers an initial capacity of 93 mA h g^{-1} at 1 C. We speculate that the longer ladder length polymer packs to

Open Access Article. Published on 29 August 2025. Downloaded on 1/22/2026 7:31:51 AM.
This article is licensed under a Creative Commons Attribution-NonCommercial 3.0 Unported Licence.

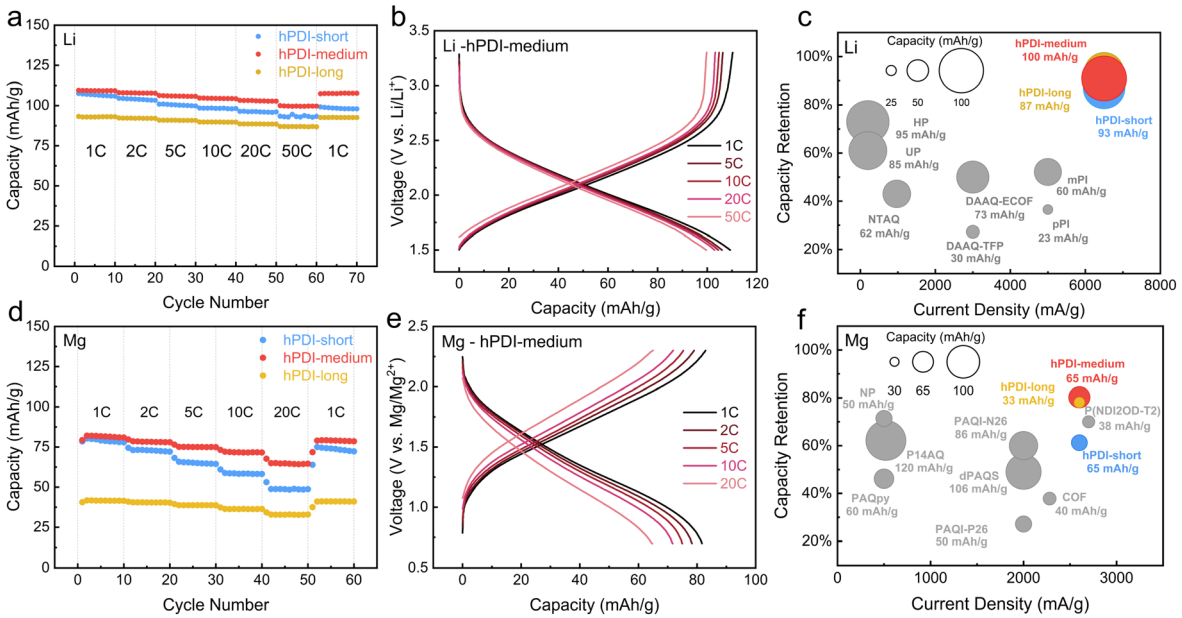

Fig. 3 (a) Rate performance of **hPDI-short**, **hPDI-medium**, and **hPDI-long** in Li batteries up to 50 C. (b) Voltage profile of the **hPDI-medium** Li battery rate performance. (c) Rate performance comparison of the hPDI-*n* series with reported polyimide-based organic polymers in Li-metal batteries. (d) Rate performance of **hPDI-short**, **hPDI-medium**, and **hPDI-long** in Mg batteries up to 20 C. (e) Voltage profile of the **hPDI-medium** Mg battery rate performance. (f) Rate performance comparison of the hPDI-*n* series with reported organic polymers in Mg-metal batteries.

occlude access to its redox active sites, lowering the capacity. There is a trade-off between ladder length and cathode performance, where **hPDI-medium** achieves high capacity at fast-charging rates even without additives commonly employed in OEMs.[25–27] Compared to other polyimide-based cathodes reported for fast-charging Li-metal batteries, **hPDI-medium** demonstrates best-in-class rate performance (Fig. 3c).[28–31] With >99.0% coulombic efficiency across all rate tests, as well as complete recovery of its initial capacity in the final 1 C cycles, hPDI-medium demonstrates excellent redox reversibility for high power applications.

Fast-charging in divalent ion systems is typically more challenging, but the hPDI series shows strong performance in Mg cells under high-rate operations (Fig. 3d and e). With a chloride-free, DME-based electrolyte, **hPDI-medium** delivers an initial capacity of 81 mA h g^{-1} at 1 C with 80% retention up to 20 C and >99.0% coulombic efficiency. **hPDI-short** delivers 80 mA h g^{-1} capacity at 1 C with 61% capacity retention at 20 C, while **hPDI-long** delivers a significantly lower initial capacity of 42 mA h g^{-1} at 1 C. Despite lower capacity, **hPDI-long** shows substantially improved capacity retention (78%) at 20 C compared to **hPDI-short**. Fig. 3f displays the capacity retention of **hPDI-medium** and **hPDI-long** at 20 C, where they outperform **hPDI-short** as well as organic polymers reported for Mg batteries.[32–37] While fast-charging capacity retention is significantly improved, the large difference in overall capacity between **hPDI-medium** and **hPDI-long** in the Mg system further points to unfavorable packing in the longest polymer, where stronger coulombic interactions inhibit access to all redox sites. The synthetic precision in OEMs is critical for Mg batteries. Beyond organic systems, the capacity retention of **hPDI-medium** under fast-charging conditions exceeds that of well-established inorganic cathodes for Li and Mg batteries (Fig. S10).[38–44]

We use SEM and HR-STEM to better understand the enhanced battery performance of **hPDI-medium** (Fig. S11 and S12). SEM images of **hPDI-short**, **hPDI-medium** and **hPDI-long** morphology. **hPDI-short** has a film-like network evenly distributed across fibers of the carbon paper electrode. **hPDI-medium** and **hPDI-long** both show large, agglomerated particles dispersed on the carbon paper fibers. HR-STEM images of the

Table 1 Rate Performance Summary of hPDI-*n* series in Li and Mg Batteries

	Li		Mg	
hPDI	Capacity at 50 C (mA h g^{-1})	Retention of 1 C capacity	Capacity at 20 C (mA h g^{-1})	Retention of 1C capacity
Short	93	86%	49	61%
Medium	100	91%	65	80%
Long	87	94%	33	78%

 © 2025 The Author(s). Published by the Royal Society of Chemistry

Open Access Article. Published on 29 August 2025. Downloaded on 1/22/2026 7:31:51 AM.
This article is licensed under a Creative Commons Attribution-NonCommercial 3.0 Unported Licence.

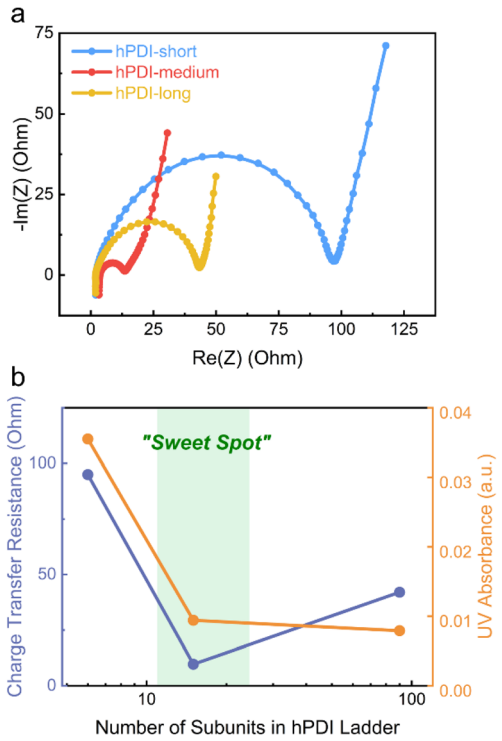

Fig. 4 (a) EIS of **hPDI-short**, **hPDI-medium**, and **hPDI-long** in Li cells. (b) The hPDI ladder length "sweet spot" for dissolution and charge transfer resistance.

cathode slurries on mesh grids provides some distinction between **hPDI-medium** and **hPDI-long** morphologies where extension into the long polymer regime gives rise to more densely agglomerated particles. The lower overall capacity of **hPDI-long**, particularly in the Mg system, can therefore be explained by its dense morphology inhibiting the diffusion of divalent Mg ions which is further supported by *b*-values indicating that charge storage is predominantly a capacitive-controlled process. Thus, we attribute enhanced performance of **hPDI-medium** to a morphology that allows access to redox sites while maintaining stability in the electrolyte.

We better understand the structure–property relationship from additional electrochemical characterization. Electrochemical impedance spectroscopy (EIS) measurements of Li batteries are shown in Fig. 4a, highlighting critical changes with increasing polymer length. The charge transfer resistance (Fig. S13) of 9.7 Ω is measured for **hPDI-medium**, lower than both **hPDI-short** (95 Ω) and **hPDI-long** (42 Ω). This lower resistance for **hPDI-medium** suggests enhanced kinetics for charge transfer, explaining its high capacity during fast-charging.[45,46] **hPDI-medium** strikes an optimal balance between insolubility and electrochemical performance (Fig. 4b). We tested an additional polymer length (40-subunit) in between **hPDI-medium** and **hPDI-long** which confirms the 15-subunit polymer as the best performing material in this series (Fig. S14).

With **hPDI-medium** identified as the sweet spot for cathode performance, we used this material for ultrahigh-rate, long-

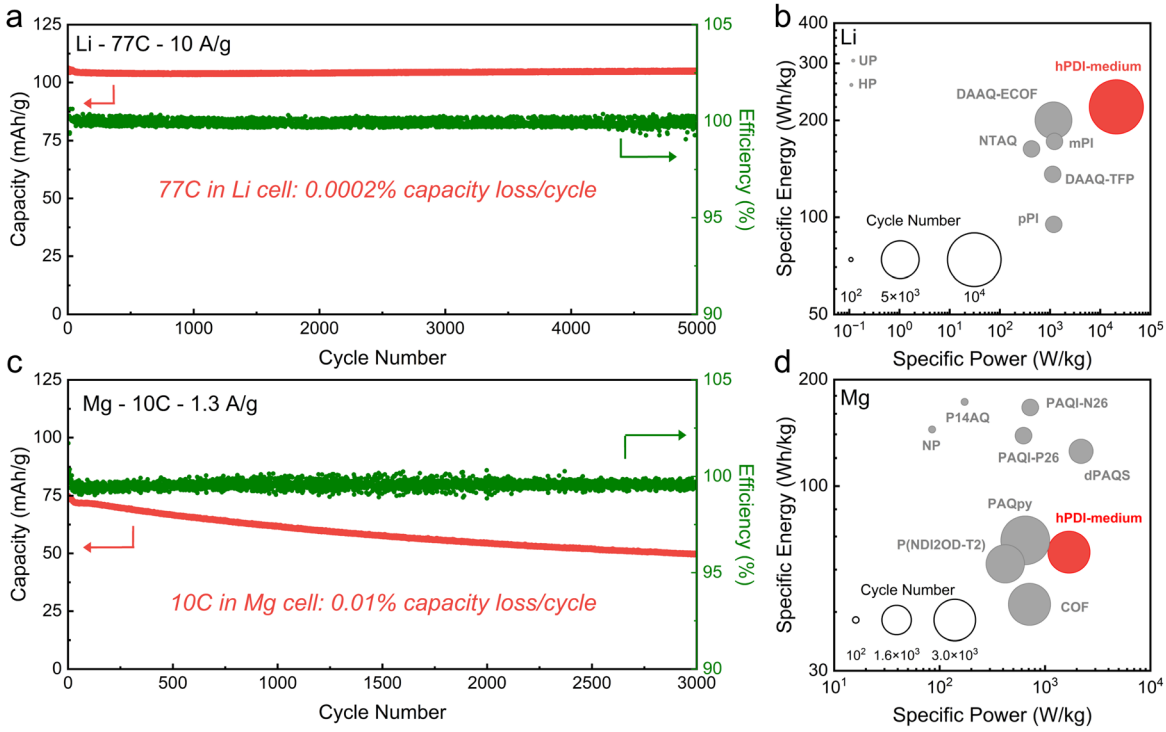

Fig. 5 Galvanostatic cycling performance of **hPDI-medium** in (a) Li batteries at 77 C for 5000 cycles and (c) Mg batteries at 10 C for 3000 cycles. Ragone plot comparing **hPDI-medium** with reported organic polymeric electrodes for (b) Li batteries and (d) Mg batteries. The circle size is the performance at maximum reported cycle number.

Open Access Article. Published on 29 August 2025. Downloaded on 1/22/2026 7:31:51 AM. This article is licensed under a Creative Commons Attribution-NonCommercial 3.0 Unported Licence.

term cycling studies in Li and Mg batteries (Fig. 5). At a 77 C rate (10 A g^{-1}) in a Li battery, **hPDI-medium** exhibits remarkable electrochemical reversibility, maintaining a coulombic efficiency >99.5% every cycle and preserving 99% of its initial 106 mA h g^{-1} capacity after 5000 cycles. There is a minuscule capacity fade of 0.0002% per cycle, underscoring its resilience to repetitive high-rate processes. Extended cycling data (Fig. S15 and S16) highlights this material's stability, demonstrating no additional capacity loss up to 10 000 total cycles. Fig. 5b presents a Ragone plot of **hPDI-medium** and other polyimide-based polymers in Li batteries (excluding OEMs with carbon nanotube additives) based on the delivered cell voltages and active electrode components.[28–31] **hPDI-medium** achieves the highest specific power (22.4 kW kg^{-1}), while maintaining a high specific energy (235 Wh kg^{-1}) after 10 000 cycles. The feasibility of **hPDI-medium** for practical applications is further demonstrated in Li cells assembled with >700% higher mass loading (2.5 mg cm^{-2}) delivering a similar capacity of 105 mA h g^{-1} at 1 C (Fig. S17).

We also observe the excellent long-term cycling stability of **hPDI-medium** in a Mg battery (Fig. 5c and S18). After 3000 cycles at 10 C (1.3 A g^{-1}), the material retains 67% of its initial 75 mA h g^{-1} capacity and maintains >99.5% coulombic efficiency. Fig. 5d is a Ragone plot comparing the long-term cycling stability and energy density of organic polymers in Mg batteries, highlighting the excellent performance of **hPDI-medium**.[32–37] **hPDI-medium** demonstrates a specific energy of 65 Wh kg^{-1} and specific power of 1.7 kW kg^{-1}, making it one of the highest power Mg batteries reported. The stability of **hPDI-medium** is also verified by *ex situ* Raman spectroscopy, confirming preserved integrity of the molecular structure after prolonged cycling (Fig. S19). The excellent performance of **hPDI-medium** with monovalent and divalent ions is promising for applications.

Conclusions

In summary, we have designed a contorted conjugated polymer that is tailored for ultrafast charging with exceptional performance in Li and Mg batteries. The synthesis allows for controlled polymer length in the hPDI-*n* series, enabling a systematic investigation of polymer length influence on cathode performance. **hPDI-medium** strikes the ideal balance of structural stability, ionic transport, and electronic conductivity to achieve outstanding rate capability and cycling stability in both monovalent and divalent ion systems. This study underscores the need to consider features at both the molecular scale (contortion) and materials scale (polymer morphology) to design high-performance organic battery materials.

Author contributions

W. L., K. H., Q. J. and C. N. conceived and designed the study. S. B. and Q. J. synthesized the compounds. W. L., K. H. and Q. J. carried out material characterizations. W. L. and K. H. collected the electrochemistry results. K. L., M. S., Q. C. and N. M. O. contributed to data interpretation and scientific discussion. K. H. and W. L. wrote the manuscript with input from all authors.

Conflicts of interest

There are no conflicts to declare.

Data availability

The data supporting this article have been included as part of the SI.

Synthesis details, materials characterization, and electrochemical data can be found in the SI. See DOI: **https://doi.org/10.1039/d5sc04900h**.

Acknowledgements

C. N. thanks Sheldon and Dorothea Buckler for their generous support. This research was supported by the National Science Foundation under Award Number CHE-2304946. We acknowledge the use of facilities and instrumentation supported by NSF through the Columbia University, MRSEC DMR-2011738. We also thank S. Okuno for help with HR-STEM measurements.

Notes and references

1 K. Qin, J. Huang, K. Holguin and C. Luo, *Energy Environ. Sci.*, 2020, **13**, 3950–3992.
2 H. Ye and Y. Li, *Energy Fuels*, 2021, **35**, 7624–7636.
3 J. Bitenc, K. Pirnat, O. Lužanin and R. Dominko, *Chem. Mater.*, 2024, **36**, 1025–1040.
4 A. Ponrouch, J. Bitenc, R. Dominko, N. Lindahl, P. Johansson and M. R. Palacin, *Energy Storage Mater.*, 2019, **20**, 253–262.
5 P. Poizot, J. Gaubicher, S. Renault, L. Dubois, Y. Liang and Y. Yao, *Chem. Rev.*, 2020, **120**, 6490–6557.
6 H. Seong, W. Nam, J. H. Moon, G. Kim, Y. Jin, H. Yoo, T. Jung, Y. Myung, K. Lee and J. Choi, *ACS Appl. Mater. Interfaces*, 2023, **15**, 58451–58461.
7 Z. Sun, H. Yao, J. Li, B. Liu, Z. Lin, M. Shu, H. Liu, S. Zhu and S. Guan, *ACS Appl. Mater. Interfaces*, 2023, **15**, 42603–42610.
8 M. Yu, X. Yu, J. Hu, C. Tang and C. Fan, *J. Energy Storage*, 2023, **74**, 109575.
9 Z. Song, Y. Qian, M. L. Gordin, D. Tang, T. Xu, M. Otani, H. Zhan, H. Zhou and D. Wang, *Angew. Chem., Int. Ed.*, 2015, **54**, 13947–13951.
10 D. Wang, Z. Zhang, Y. Hao, H. Jia, X. Shen, B. Qu, G. Huang, X. Zhou, J. Wang, C. Xu and F. Pan, *Adv. Funct. Mater.*, 2024, **34**, 2410406.
11 J. Song, E. Sahadeo, M. Noked and S. B. Lee, *J. Phys. Chem. Lett.*, 2016, **7**, 1736–1749.
12 C. You, X. Wu, X. Yuan, Y. Chen, L. Liu, Y. Zhu, L. Fu, Y. Wu, Y.-G. Guo and T. Van Ree, *J. Mater. Chem. A*, 2020, **8**, 25601–25625.
13 M. Mao, T. Gao, S. Hou and C. Wang, *Chem. Soc. Rev.*, 2018, **47**, 8804–8841.
14 A. H. Epstein and S. M. O'Flarity, *J. Propul. Power*, 2019, **35**, 572–582.

 © 2025 The Author(s). Published by the Royal Society of Chemistry

Open Access Article. Published on 29 August 2025. Downloaded on 1/22/2026 7:31:51 AM.
This article is licensed under a Creative Commons Attribution-NonCommercial 3.0 Unported Licence.

15 V. Königer and V. Knoblauch, *Appl. Sci.*, 2023, **13**, 8848.
16 M. Dixit, A. Bisht, R. Essehli, R. Amin, C.-B. M. Kweon and I. Belharouak, *ACS Energy Lett.*, 2024, **9**, 934–940.
17 M. A. Rendón, C. D. Sánchez R., J. Gallo M. and A. H. Anzai, *J. Control Autom. Electr. Syst.*, 2021, **32**, 1244–1268.
18 Z. Jin, Q. Cheng, S. T. Bao, R. Zhang, A. M. Evans, F. Ng, Y. Xu, M. L. Steigerwald, A. E. McDermott, Y. Yang and C. Nuckolls, *J. Am. Chem. Soc.*, 2022, **144**, 13973–13980.
19 S. T. Bao, Y. Hong, H. Jiang, L. T. Lackovic, S. Louie, D. Xu, F. Ng, N. Olsen, X. Zhu, M. L. Steigerwald, M. Delor, C. Nuckolls and Q. Jiang, *Angew. Chem., Int. Ed.*, 2025, **64**, e202508426.
20 S. R. Peurifoy, J. C. Russell, T. J. Sisto, Y. Yang, X. Roy and C. Nuckolls, *J. Am. Chem. Soc.*, 2018, **140**, 10960–10964.
21 J. C. Russell, V. A. Posey, J. Gray, R. May, D. A. Reed, H. Zhang, L. E. Marbella, M. L. Steigerwald, Y. Yang, X. Roy, C. Nuckolls and S. R. Peurifoy, *Nat. Mater.*, 2021, **20**, 1136–1141.
22 Z. Jin, Q. Cheng, A. M. Evans, J. Gray, R. Zhang, S. T. Bao, F. Wei, L. Venkataraman, Y. Yang and C. Nuckolls, *Chem. Sci.*, 2022, **13**, 3533–3538.
23 T. Schoetz, L. W. Gordon, S. Ivanov, A. Bund, D. Mandler and R. J. Messinger, *Electrochim. Acta*, 2022, **412**, 140072.
24 H. Lindström, S. Södergren, A. Solbrand, H. Rensmo, J. Hjelm, A. Hagfeldt and S.-E. Lindquist, *J. Phys. Chem. B*, 1997, **101**, 7717–7722.
25 J. F. Baumgärtner, K. V. Kravchyk and M. V. Kovalenko, *Adv. Energy Mater.*, 2025, **15**, 2400499.
26 G. Wang, N. Chandrasekhar, B. P. Biswal, D. Becker, S. Paasch, E. Brunner, M. Addicoat, M. Yu, R. Berger and X. Feng, *Adv. Mater.*, 2019, **31**, 1901478.
27 J. Xie, Z. Wang, Z. J. Xu and Q. Zhang, *Adv. Energy Mater.*, 2018, **8**, 1703509.
28 S. Wang, Q. Wang, P. Shao, Y. Han, X. Gao, L. Ma, S. Yuan, X. Ma, J. Zhou, X. Feng and B. Wang, *J. Am. Chem. Soc.*, 2017, **139**, 4258–4261.
29 R. R. Kapaev, A. G. Scherbakov, A. F. Shestakov, K. J. Stevenson and P. A. Troshin, *ACS Appl. Energy Mater.*, 2021, **4**, 4465–4472.
30 P. Sharma, D. Damien, K. Nagarajan, M. M. Shaijumon and M. Hariharan, *J. Phys. Chem. Lett.*, 2013, **4**, 3192–3197.
31 Z. Ba, Z. Wang, M. Luo, H. Li, Y. Li, T. Huang, J. Dong, Q. Zhang and X. Zhao, *ACS Appl. Mater. Interfaces*, 2020, **12**, 807–817.
32 T. Bančič, J. Bitenc, K. Pirnat, A. Kopač Lautar, J. Grdadolnik, A. Randon Vitanova and R. Dominko, *J. Power Sources*, 2018, **395**, 25–30.
33 H. Dong, Y. Liang, O. Tutusaus, R. Mohtadi, Y. Zhang, F. Hao and Y. Yao, *Joule*, 2019, **3**, 782–793.
34 Y. Ding, D. Chen, X. Ren, Y. Cao and F. Xu, *J. Mater. Chem. A*, 2022, **10**, 14111–14120.
35 R. Sun, S. Hou, C. Luo, X. Ji, L. Wang, L. Mai and C. Wang, *Nano Lett.*, 2020, **20**, 3880–3888.
36 X. Song, X. Xue, H. Xia, L. Jin, A. Tao, Y. Wang, J. Liang, Y. Liu, P. Zhang, Z. Tie, Y. Long and Z. Jin, *Energy Storage Mater.*, 2023, **55**, 426–435.
37 X. Ren, D. Tao, S. Cui, T. Li, Y. Cao and F. Xu, *Energy Storage Mater.*, 2023, **63**, 102992.
38 T. Fu, Y. Li, Z. Yao, T. Guo, S. Liu, Z. Chen, C. Zheng and W. Sun, *Small*, 2024, **20**, 2402339.
39 F. Cheng, X. Zhang, Y. Qiu, J. Zhang, Y. Liu, P. Wei, M. Ou, S. Sun, Y. Xu, Q. Li, C. Fang, J. Han and Y. Huang, *Nano Energy*, 2021, **88**, 106301.
40 T. Shi, F. Liu, W. Liu, H. Wang, K. Han, C. Yang, J. Wu, J. Meng, C. Niu, C. Han and X. Wang, *Nano Energy*, 2024, **123**, 109410.
41 V. Ramar, C. Pszolla, M. Rapp, M. Borck and L. Zinck, *J. Electrochem. Soc.*, 2020, **167**, 070521.
42 F. Wang, H. Hua, Y. Zhuang, J. Wu, J. Zeng and J. Zhao, *Adv. Funct. Mater.*, 2025, **35**, 2414181.
43 Y. Cheng, Y. Shao, V. Raju, X. Ji, B. L. Mehdi, K. S. Han, M. H. Engelhard, G. Li, N. D. Browning, K. T. Mueller and J. Liu, *Adv. Funct. Mater.*, 2016, **26**, 3446–3453.
44 R. Sun, C. Pei, J. Sheng, D. Wang, L. Wu, S. Liu, Q. An and L. Mai, *Energy Storage Mater.*, 2018, **12**, 61–68.
45 H. Wu, K. Wang, Y. Meng, K. Lu and Z. Wei, *J. Mater. Chem. A*, 2013, **1**, 6366.
46 C. Li, M. Yin, Z. He, W. Tao, Y. Jia, H. Yu, Q. Zeng, J. H. Xin, D. Wang and X. Liu, *J. Power Sources*, 2022, **542**, 231824.